NMR MICROSCOPY FOR FLUID IMAGING AT PORE SCALE IN RESERVOIR ROCK

By Daryl A. Doughty and Liviu Tomutsa

For presentation at
33rd Annual Symposium of the
Society of Professional Well Log Analysts
Co-sponsored by the Society of Core Analysts
Oklahoma City, Oklahoma
June 14-17, 1992

IIT Research Institute
National Institute for Petroleum and Energy Research
P.O. Box 2128
220 N. Virginia Avenue
Bartlesville, Oklahoma 74005
Telephone 336/2400

NMR MICROSCOPY FOR FLUID IMAGING AT PORE SCALE IN RESERVOIR ROCK

by Daryl A. Doughty and Liviu Tomutsa

ABSTRACT

Fluids in reservoir rocks exhibit nuclear magnetic resonance (NMR) characteristics more like those of solids than liquids. Very short T_2 relaxation times and broad natural line widths are caused primarily by paramagnetic components in the rock matrix. These characteristics place severe constraints on the NMRI methodology that can be used to obtain high-resolution, pore-scale images of fluid in reservoir rock. Because the relaxation and line broadening are not caused by dipolar coupling, multiple-pulse line narrowing techniques developed for NMRI in solids will not work. Very strong imaging gradients (75 to 150 Gauss/cm) are required to achieve meaningful voxel resolutions which severely limit the rapid switching of gradients required for most NMR slice-imaging techniques. An NMRI protocol based on 3D back-projection is presented and its advantages (high resolution in three dimensions, multi-planar slice selection) and limitations (RF pulse power, acquisition time, data file size, computational demands) are discussed. Using this protocol, images of two-phase fluid systems in rock samples have been obtained using 65536 projections and 256 complex points per projection about spherical coordinate space. Resolutions as high as 25 microns per pixel have been obtained. A brief discussion of sample preparation requirements is presented. Results are presented showing one- and two-phase fluid distributions in reservoir rock at the pore level.

INTRODUCTION

The development of nuclear magnetic resonance (NMR) imaging from high-resolution NMR spectroscopy is straightforward in concept. In NMR spectroscopy, the sample is placed in a highly homogeneous magnetic field. All NMR-active nuclei of a given species, for example protons in water, will experience the same magnetic field and resonate at the same frequency, resulting in a sharp peak for water in the NMR spectrum, but no information is obtained to spatially differentiate one water molecule from another. If a linear gradient in magnetic field intensity is superimposed on the homogeneous field, then water protons on the side of the sample exposed to the lower fields will resonate at lower frequencies and the protons exposed to the higher fields will resonate at higher frequencies. What will be observed in the NMR spectrum will be a projection of the summed intensity from water protons in perpendicular planes at each position along the diameter of the sample in the direction of the gradient field from lowest to highest frequency. Figure 1 illustrates this projection process. By changing the orientation of the gradient in three-dimensional (3D) space in a regular manner, information about the location of all water protons in the sample can be obtained, and an "image" of the water distribution in selected planes from the sample can be displayed. This NMR imaging process was first developed in 1973 (Lauterbur, 1973.) In the intervening 19 years, many developments have occurred in the

techniques used for manipulating gradients, acquiring data, and processing images to obtain desired results, and NMR imaging has been extended to a wide variety of applications, from medicine to biological research to solid state and many other research areas (Dumoulin, 1987; Kuhn, 1990.)

In the area of petroleum production research and reservoir characterization, NMR imaging (NMRI), like computerized X-ray tomography (CT) imaging, is a nondestructive imaging technology transferred from the medical field to the petroleum industry to image fluids within cores. Since the mid-1980's, increasing numbers of applications and developments of NMRI in petroleum research have occurred (Rothwell and Vinegar, 1985; Baldwin and Yamanashi, 1986; Hall and Rajanayagam, 1987; Doughty and Maerefat, 1989; Edelstein, et al., 1988; Mahmood, et al., 1990; Tutunjian, et al., 1991; Robinson and Edelstein, 1991; Chang and Edwards, 1991; Chardaire-Riviere and Roussel, 1991.) The issues to be addressed by NMRI for petroleum research are: (a) spatial resolution, (b) image acquisition and processing techniques, and (c) differentiation of oil, water and gas phases within cores. The high resolution achievable allows visualization of the effect of rock/fluid interaction on oil and water distributions within pore spaces of reservoir rocks. Such a capability is of direct help in understanding oil displacement processes taking place at the pore level and is essential in understanding the mechanisms of various oil recovery processes.

The spin-spin relaxation time (T_2) controls the amount of time that usable NMR signals persist after the radio-frequency (RF) pulse. Fluids in many reservoir rocks exhibit NMR characteristics more like those of solids than liquids including very short T_2 relaxation times and broad natural line widths caused primarily by paramagnetic components in the rock matrix. After about five T_2 periods, the measurable signal disappears. At a proton frequency of 270 MHz, corresponding to the 6.34 T magnetic field, the T_2 times of fluids in typical porous rock are reduced to the 0.2 to 1 msec range (the shorter times are for rock containing clays or other materials containing many paramagnetic species such as Fe or Mn). To use NMRI for imaging these samples would require RF pulse sequences which are shorter than 5 msec. This eliminates most pulse sequences which image a "slice" of the sample by using a spin-echo method with a selective RF pulse of narrow bandwidth which lasts several milliseconds. Also, the three X, Y, and Z gradients must be turned on and off sequentially which adds 5 to 6 millisec more to these sequences. Very strong imaging gradients (75 to 150 Gauss/cm) are required to achieve meaningful voxel resolutions which severely limit the rapid switching of gradients required for most NMR slice-imaging techniques.

A three-dimensional (3D) projection-reconstruction NMRI method does not require this rapid gradient response as the gradients are turned on and a short RF pulse having a broad bandwidth irradiates the sample in the presence of the gradient which is then turned off after the signal is acquired. The advantage is that the NMR signal can be acquired immediately after the RF pulse (about 5 microsec) or after a short echo period (1 to 2 msec) so that a strong signal is available. The disadvantages are that the entire sample is irradiated at once, generating very large data files and requiring longer sampling times and larger data processing periods. Also a short, powerful RF

pulse is required to excite the entire sample adequately in the presence of the strong gradient if an echo sequence is used.

EQUIPMENT DESCRIPTION

The block diagram of the NMR spectrometer incorporating the different components for imaging is shown in schematic form in Figure 2. The NMR spectrometer block represents the standard high-resolution instrument (JEOL GX270 wide bore system) with the RF components that transmit and detect the NMR signals and the pulse programmer that controls the timing of the signal acquisition process.

The 25-MHz 386-PC block represents the added high-speed data acquisition unit, capable of acquiring data in two channels at 1 MHz, and the imaging gradient switching and amplitude control unit. Also shown in Figure 2 are the gradient amplifiers, the gradient coil system, and the sample probe which contains the RF coils which surround the sample and transmit the NMR frequencies to the sample and receive the image signals.

The 33-MHz 386-PC block shown in Figure 2 contains a RISC coprocessor board based on the Intel i860 cpu running the projection reconstruction image processing software. A 256 x 256 x 256 image file takes slightly more than 5 hours to process with the coprocessor board. The software is designed to permit the processing of a subset of the data for faster processing of selected regions of interest. The data files are transferred between the two 386 computers through the parallel printer ports using commercially available software. This permits the transfer of the large image data files to the processing computer in only a few minutes. For mass storage and archiving, a 44 Mbyte removable cartridge drive and a 2.3-Gbyte 8-mm tape drive unit are used for the processing computer. Several image files can be stored on one cartridge, while several hundred can be stored on the 8-mm tape cassette.

To achieve spatial resolutions in the 20-micron range, a gradient coil assembly was designed and constructed to produce imaging gradients up to 170 Gauss/cm. The schematic drawing of the gradient coils with the location of the probe and the magnetic field direction is shown in Figure 3. The gradient assembly was designed to fit over the standard NMR sample probes as well as the new sample probe described below. At the high gradient strength of this coil assembly, imaging an object 1 cm across using the proton frequency of the NMR spectrometer of 270 MHz would require a bandwidth of 724,000 Hz, about seven times larger than the current NMR spectrometer bandwidth, which is only 100,000 Hz. Figure 3 shows schematically the arrangement of the gradient coils and RF probe.

A new NMRI imaging probe was also designed and constructed for high resolution imaging. The RF coil is more efficient and can generate the shorter 90-degree RF pulses required for projection reconstruction NMRI at the higher gradients which can be attained with the new gradient assembly described above. The new probe design utilizes a horizontal sample orientation with solenoidal RF coils rather than the vertical saddle-coil arrangement found in the standard probes. The probe circuit displays a good Q factor (110) and a suitable tuning range which covers both the proton and the

fluorine frequencies of 270.2 MHz and 254.2 MHz, respectively. Using a high-power amplifier, 90-degree RF pulses as short as 2.0 microsec have been obtained.

IMAGING PROCESSING AND DISPLAY

Two basic methods are available for reconstructing the 3D image from the raw projection data in projection reconstruction NMRI: (1) a direct approach based on the application of the Radon transform in three dimensions and (2) a two-stage reconstruction involving two successive applications of standard 2-D Radon transforms (Chen, 1980.) The two-stage method adapted from standard CT programs is more efficient involving approximately $2N^4$ operations to reconstruct the entire 3D image where N is the cubical dimension of the image. The major shortcoming in this approach is the impossibility of reconstructing only part of the image; the complete image must be reconstructed. With the direct approach, reconstruction of the complete 3D image involves approximately N^5 operations which would require much more time. However, the direct approach does permit a partial reconstruction of selected regions of the image, for example a single slice view of arbitrary orientation, or a reduced volume image using only a subset of the raw data. Because the acquisition of the data is the limiting factor, imaging the central volume of a sample at high resolution would be possible with a reduced number of raw projections using the direct approach. FORTRAN programs implementing both reconstruction algorithms have been modified to be compatible with our data acquisition and imaging format (Huesman, et al., 1977; Shepp, 1980.) The timing of the pulse sequence is shown in Figure 4.

The three dimensional arrays of the fluid concentrations in the pores are visualized on an Apple Macintosh IIfx desktop computer, by using a data display and analysis software package commercially available. This software package allows viewing of any 3D object sections along planes parallel to XY, XZ, and YZ planes as well as rotation of the 3D object around the x, y, and z axis. Various color tables as well as a gray scale are available for the data display. By stacking up 2-D sections and using the transparency mode, which associates background color to selected data value ranges, one can display 3D distributions of physical properties within the value of interest.

EXPERIMENTAL

For small scale studies by NMRI, small cores (4 to 5 mm diameter, 6 to 8 mm long) are needed. A microcoring apparatus was built by modifying a small bench-model drill press for use with 1/4 inch and 5/16 inch miniature diamond core drills. The 1/4 inch core drill produces a core plug approximately 4 mm in diameter and the 5/16 inch core drill produces a core plug approximately 5 mm in diameter. Several sample holders were machined out of Teflon which center the small plugs in the NMRI sample probe. Other flow cells were made using Teflon end pieces and Teflon shrink tubing with 1/16 inch Teflon tubing to carry fluids to the cell while mounted in the probe. Because of the small size of these plugs and the long time required for data acquisition, it is very difficult to image dynamically a realistic flood experiment and obtain a meaningful image of the resulting fluid distributions

at various stages of the experiment. Instead determinations of fluid distributions were made only for single phase or for end points (residual oil and residual brine). Floods were carried out in 1.5 inch diameter core plugs and small samples were taken for NMRI pore level imaging from the large plug in regions identified by CT as being of interest.

NMRI MEASUREMENTS AND RESULTS

First, for calibration purpose, the NMRI work has been focused on increasing the resolution of the system down to 25 microns on sample beadpacks prepared from polymer microspheres. Using polymer beads having a size range of 250 to 350 microns, a bead pack was made in a sample cell with a diameter of 3 mm and a length of 6 mm and saturated under vacuum with water. NMRI images of the bead pack have been obtained at 128 x 128 x 128 pixels and 256 x 256 x 256 pixels. The pixel size at the lower resolution is 30 microns while at the higher resolution a pixel size of 15 microns was obtained. Figure 5 shows an NMRI image of the beadpack at the higher resolution. The circular silhouettes of the beads can clearly be seen with the water which occupies the voids between the beads appearing as the brighter areas between the beads.

NMRI images of fluids in a sandstone rock sample at high resolution have also been obtained. The sample was a small plug of Bentheim sandstone 5.3 mm in diameter and 8 mm long. The Bentheim plug was initially saturated with brine under vacuum. The brine contained 0.002M $MnCl_2$ as a relaxation agent, 1.25% NaI and 0.25% NaCl. Longitudinal relaxation time (T_1) measurements showed the aqueous phase had a T_1 time of 80 milliseconds. Several images of the aqueous phase were made at pixel resolutions of 128 x 128 x 128 and 256 x 256 x 256. A gradient strength of 75 Gauss/cm was used. At the highest resolution the pixel size was 40 microns in the cross- sectional views with 40 microns along the axis. These are the highest resolution images obtained to date of fluids in sandstone. Soltrol mineral oil with the viscosity adjusted to 5 cp was injected into the water-saturated Bentheim plug (2 mL or about 100 pore volumes was used.) The injection was done under gravity flow with a pressure head of about 8 feet. The T_1 measurement of the oil phase gave a value of 523 milliseconds. Two images of the plug were made at a pixel resolution of 256 x 256 x 256: one showing the total fluid distribution and the second showing the oil phase using a longer TE period imaging sequence to null the brine phase signal. In Figure 6, three images of fluid distribution in the pores are shown at initial oil saturation: the total fluid image (top), which defines the pore geometry and connectivity, the brine phase (middle), and the oil phase (bottom). The brine phase was obtained by subtraction of the oil phase image from the total fluid image By comparing the three images the relative position of the oil and brine can be defined within the pore spaces. Notice the water appears as small isolated droplets with virtually the entire pore space being filled with the oil phase. In Figure 7, three images of fluid distribution in the pores are shown at residual oil saturation, after water flooding the micro core: the total fluid image (top), the brine phase (middle), and the oil phase (bottom). Notice that in some cases the oil seems to be filling pores in a connected fashion while in other cases the oil droplets float in the center of the pore completely surrounded by water. Because of the longer T_1

value for the oil and the lower signal/noise ratio for the oil only signal each of these images took approximately 48 hours to acquire.

In Figure 8, the brine filled pores of a sample of Bartlesville sandstone are shown. The image was generated for a micro plug 5.3 mm diameter and 7 mm long, saturated with the same brine as used for the Bentheimer sample. Because the natural line width of the brine was 2.5 times wider in this sample, a stronger gradient and a wider acquisition bandwidth was used to obtain the image. The final pixel resolution was the same as that used for the Bentheimer images.

CONCLUSIONS

A high field NMR spectrometer has been modified to generate images of oil and water in pores of sandstone samples with spatial resolution as high as 40 microns.

Using an NMRI protocol based on 3D back-projection many of the imaging constraints associated with the NMR slice imaging techniques have been overcome in generating pore level fluid images.

A new technique has been developed to prepare and contain micro plugs for imaging purposes.

Due to the long time necessary for image acquisition, only end point fluid saturations can be imaged at present.

ACKNOWLEDGMENTS

This work was supported by the U.S. Department of Energy under Cooperative Agreement DE-FC22-83FE60149. Bob Lemmon and Alex Crawley of the DOE Bartlesville Project Office are acknowledged for their help in conducting this work. The authors thank M. Madden, T. E. Burchfield, M. K. Tham and Bill Linville, all of NIPER for their reviews of this paper.

REFERENCES

Baldwin, B. A. and Yamanashi, W. X. (1986), "Detecting Fluid Movement and Isolation in Reservoir Cores Using Medical NMR Imaging Techniques," Presented at the Fifth SPE/DOE Symposium on Enhanced Oil Recovery, Tulsa, Oklahoma, 20-23 April, SPE/DOE Paper 14884.

Chang, C. T. and Edwards, C. M. (1991), "Proton MR Two-Component Chemical Shift Imaging of Fluids in Porous Media," Presented at the Fifth Annual Technical Conference, Society of Core Analysts, New Orleans, Louisiana, 21-21 August, SCA paper 9114.

Chardaire-Riviere, C. and Roussel, J.-C. (1991), "Use of a High Magnetic Field to Visualize Fluids in Porous Media by MRI," Presented at the Fifth Annual Technical Conference, Society of Core Analysts, New Orleans, Louisiana, 21-21 August, SCA paper 9112.

Chen, C.-N. (1980), "Direct Three-Dimensional Image Reconstructions from Plane Integrals and Their Applications in Nuclear Magnetic Resonance Zeugmatography," Part 1 of Ph.D. dissertation, Chemistry Department, SUNY Stony Brook.

Doughty, D. A. and Maerefat, N. L. (1989), "Preliminary Transformation of an NMR Spectrometer into an NMR Imager for Evaluating Fluid Content and Rock Properties of Core Samples," *Log Analyst*, Mar.-Apr., p. 78.

Dumoulin, C. L. (1987), "Nuclear Magnetic Resonance Imaging," *Spectroscopy*, v. 2, no. 1, p. 32.

Edelstein, W. A., Vinegar, H. J., Tutunjian, P. N., Roemer, P. B., and Mueller, O. M. (1988), "NMR Imaging for Core Analysis," Presented at the 63rd Annual Technical Conference and Exhibition of the Society of Petroleum Engineers, Houston, Texas, 2-5 October., SPE paper 18272.

Hall, L. D. and Rajanayagam, V. (1987), "Thin-Slice, Chemical Shift Imaging of Oil and Water in Sandstone Rock at 80 MHz," *J. Magn. Reson.*, v. 74, p. 139.

Huesman, R. H., Gullberg, G. T., Greenbery, W. L., and Budinger, T. F. (1977), "Users Manual: Donner Algorithms for Reconstruction Tomography," Donner Laboratory, Biology and Medicine Division, Lawrence Berkeley Laboratory, Univ. of Calif., October.

Kuhn, W. (1990), "NMR Microscopy - Fundamentals, Limits and Possible Applications," *Angew. Chem. Int. Ed. Engl.*, v. 29, no. 1, p. 1.

Lauterbur, P. C. (1973), "Image Formation by Induced Local Interactions: Examples Employing Nuclear Magnetic Resonance," *Nature*, v. 242, p. 190.

Mahmood, S. M., Doughty, D. A., Tomutsa, L., and Honarpour, M. (1990), "Pore Level Fluid Imaging Using High Resolution Nuclear Magnetic Resonance Imaging and Thin Slab Micromodels," Presented at the Fourth Annual Technical Conference of the Society of Core Analysts, Dallas, Texas, 13-15 Aug., SCA paper 9024.

Robinson, M. A. and Edelstein, W. A. (1991), "Fluid Velocities in Oil Cores During Water Injection," Presented at the Fifth Annual Technical Conference, Society of Core Analysts, New Orleans, Louisiana, 21-21 August, SCA paper 9113.

Rothwell, W. P. and Vinegar, H. J. (1985), "Petrophysical Applications of NMR Imaging," *Applied Optics*, v. 24, p. 3969.

Shepp, L. A. (1980), "Computerized Tomography and Nuclear Magnetic Resonance," *J. Comput. Assist. Tomogr.*, v. 4, no. 1, p. 94.

Tutunjian, P. N., Vinegar, H. J., and Ferris, J. A. (1991), "Nuclear Magnetic Resonance Imaging of Sodium-23 in Cores," Presented at the Fifth Annual Technical Conference, Society of Core Analysts, New Orleans, Louisiana, 21-21 August, SCA paper 9111.

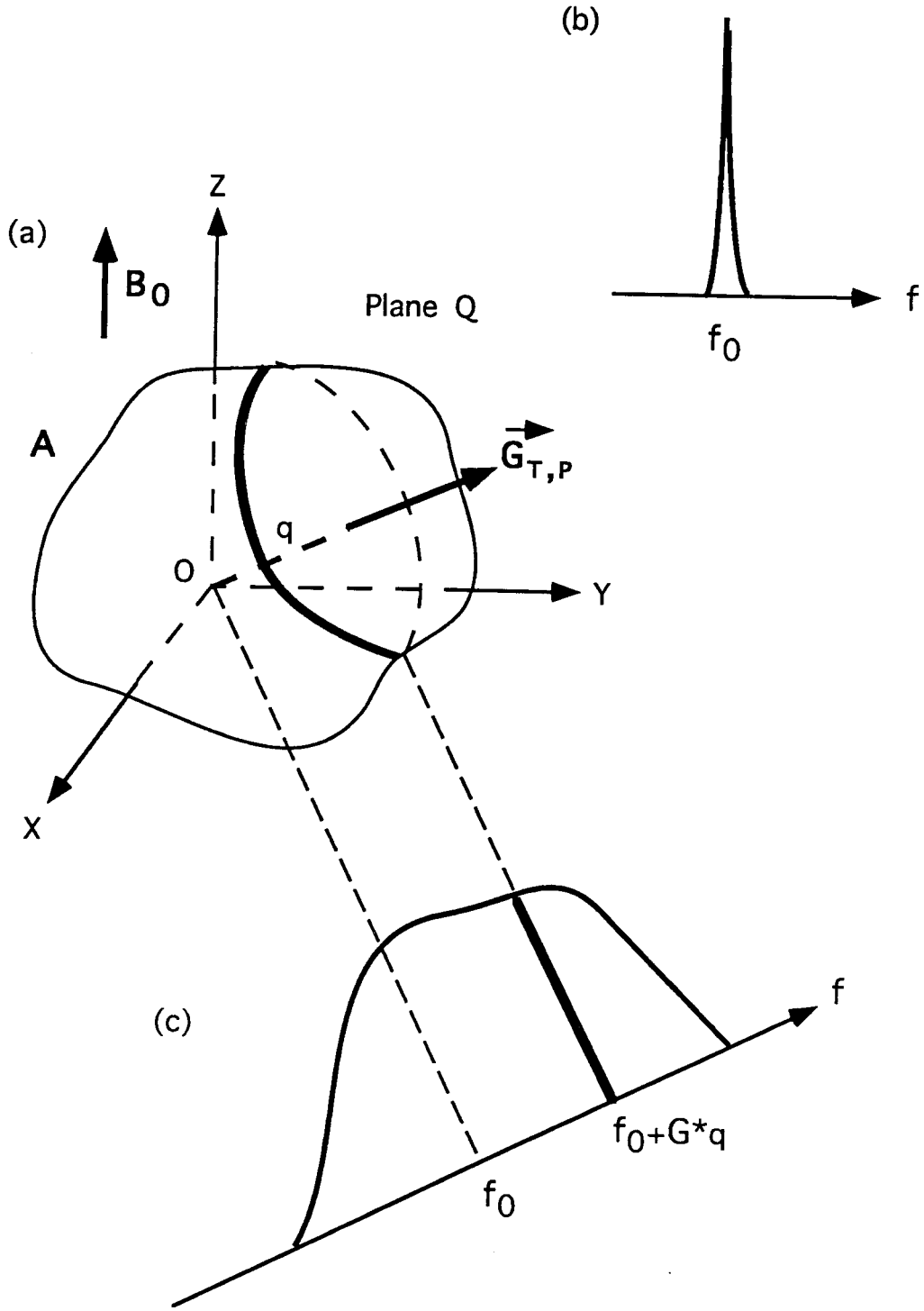

Figure 1. (a) A three-dimensional object subject to a main magnetic field B_0 and a magnetic field gradient $G_{T,P}$; (b) Conventional NMR spectrum in the absence of the field gradient and for identical nuclei; (c) NMR spectrum of the object for a non zero field gradient applied in the direction $G_{T,P}$.

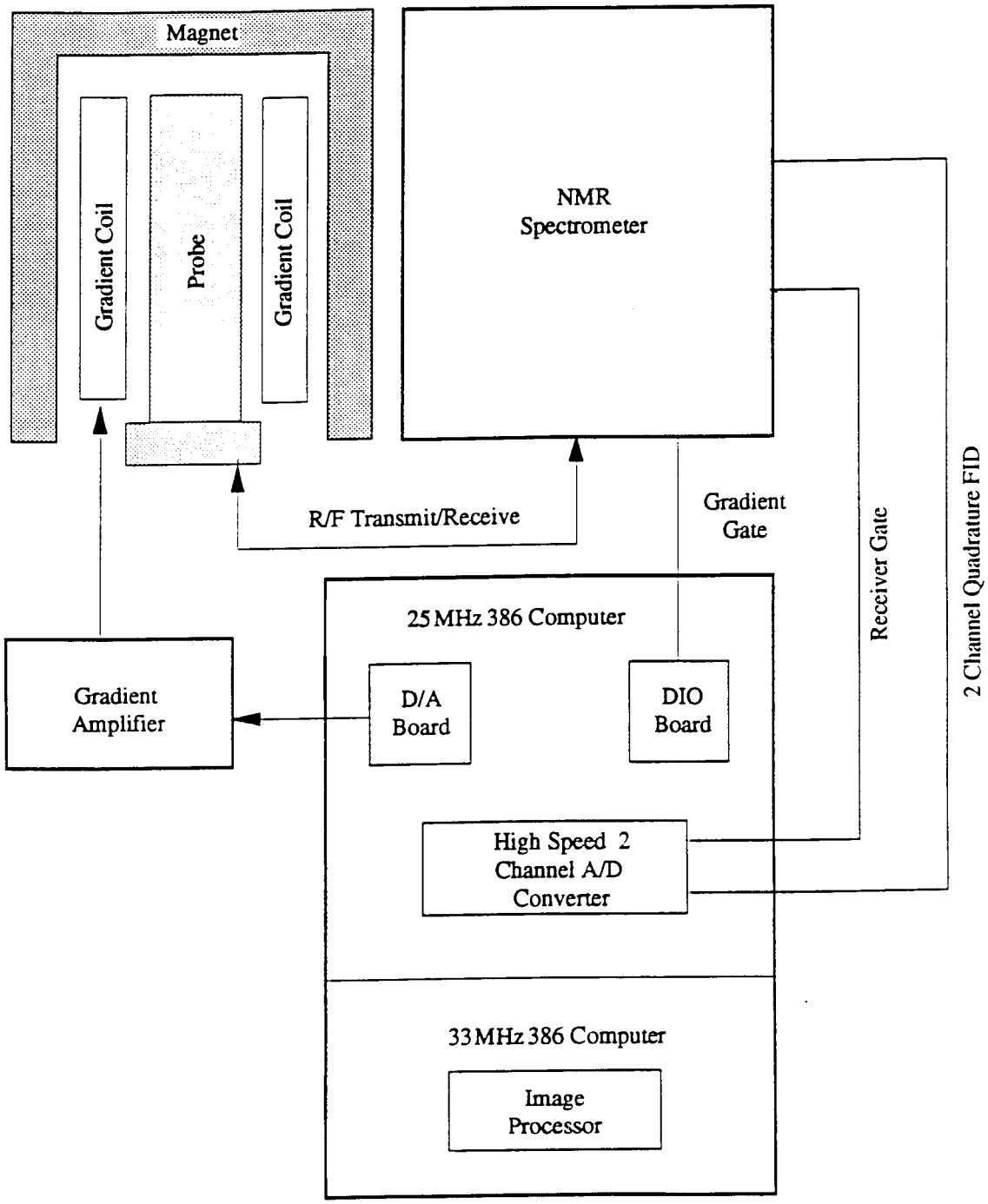

Figure 2. Block diagram of the high resolution NMRI apparatus.

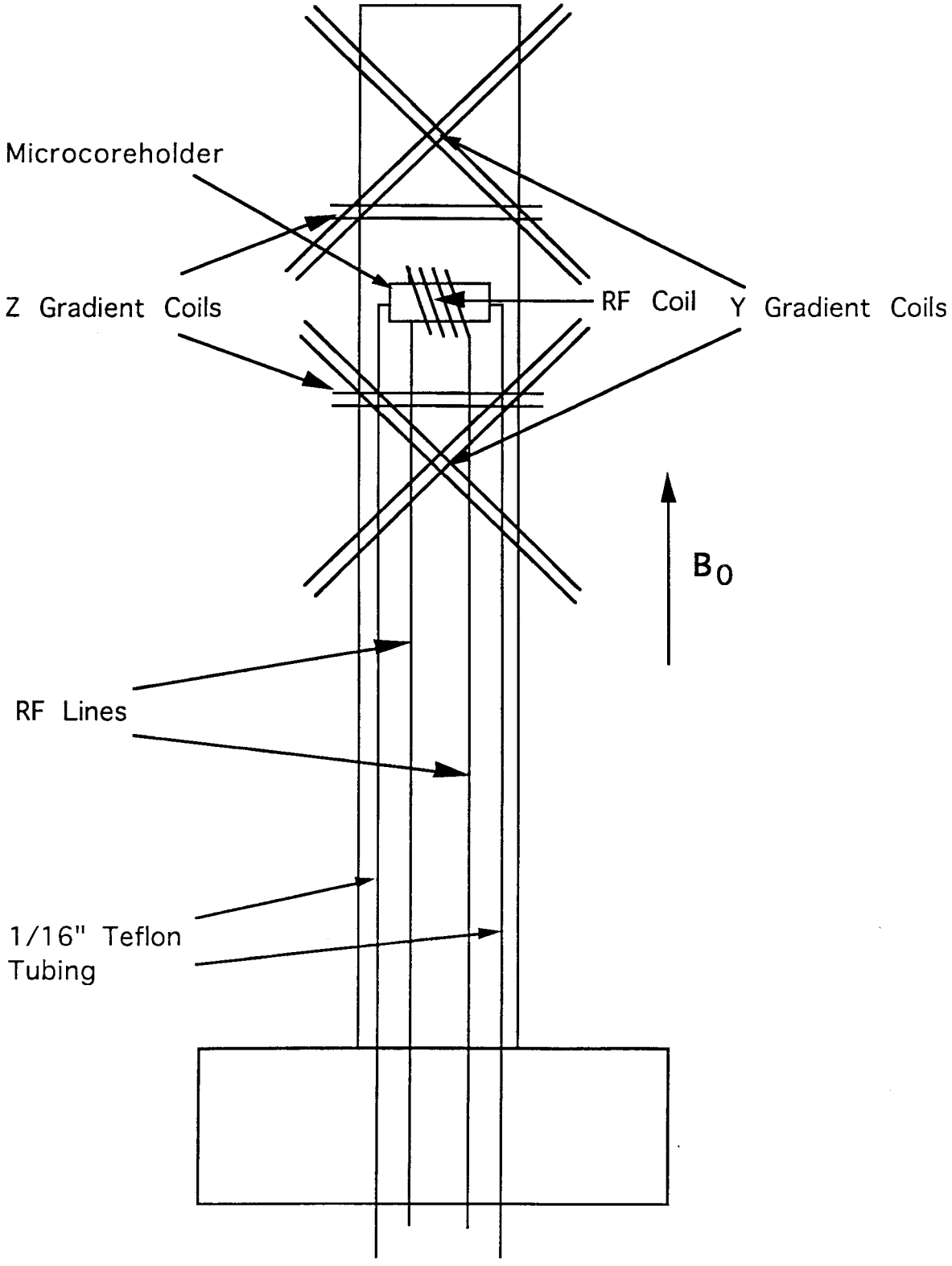

Figure 3. Schematic drawing of the gradient coils with the location of the probe and the magnetic field direction

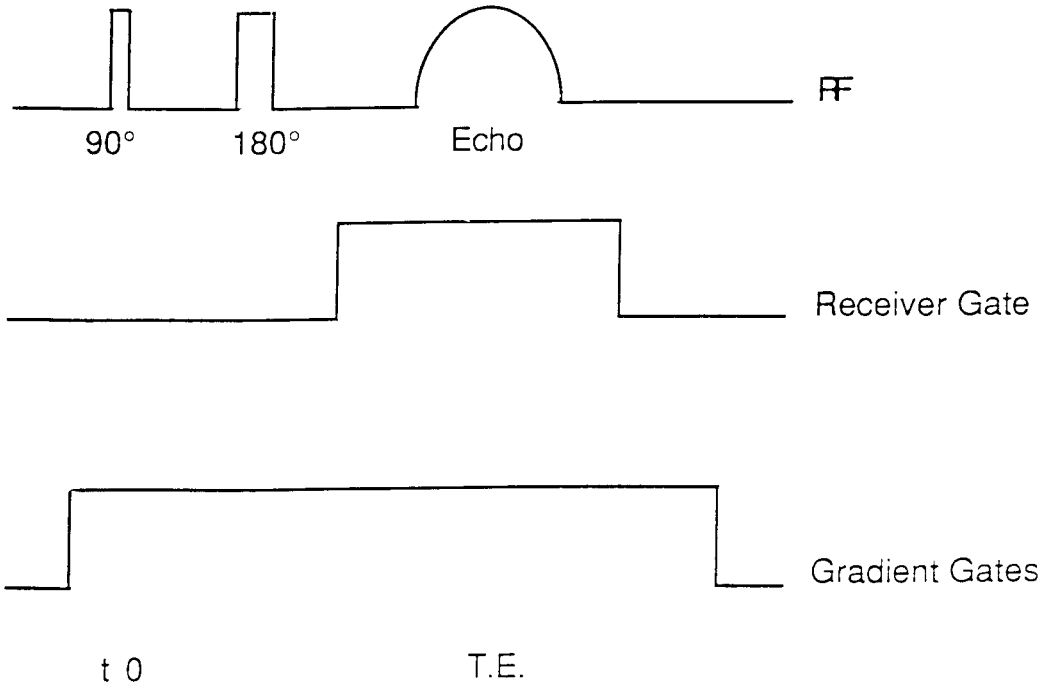

Figure 4. Pulse time sequence

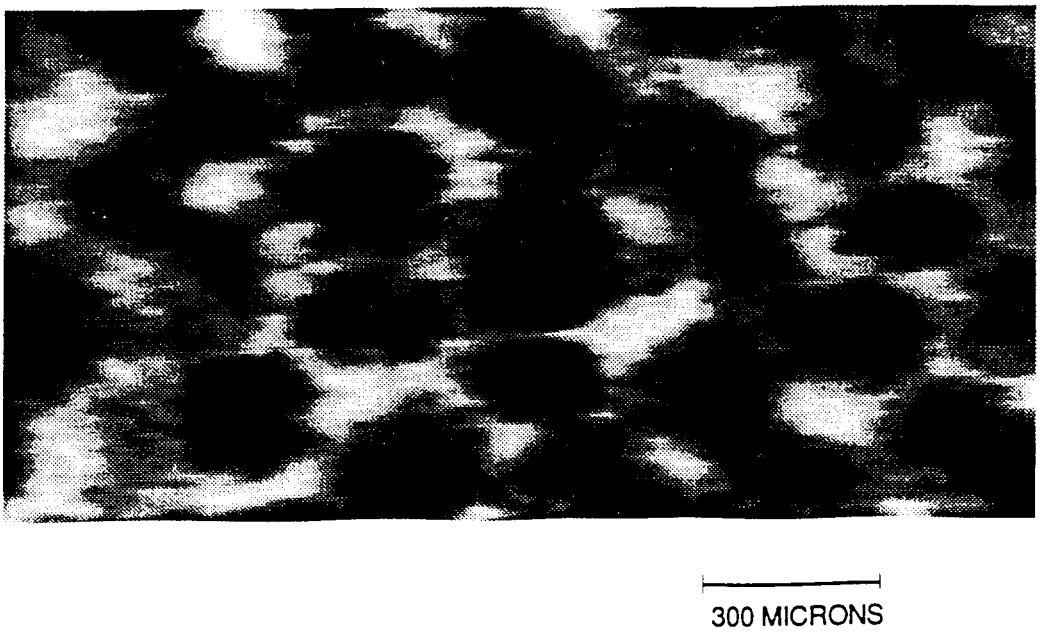

Figure 5. High resolution NMRI image of water in bead pack

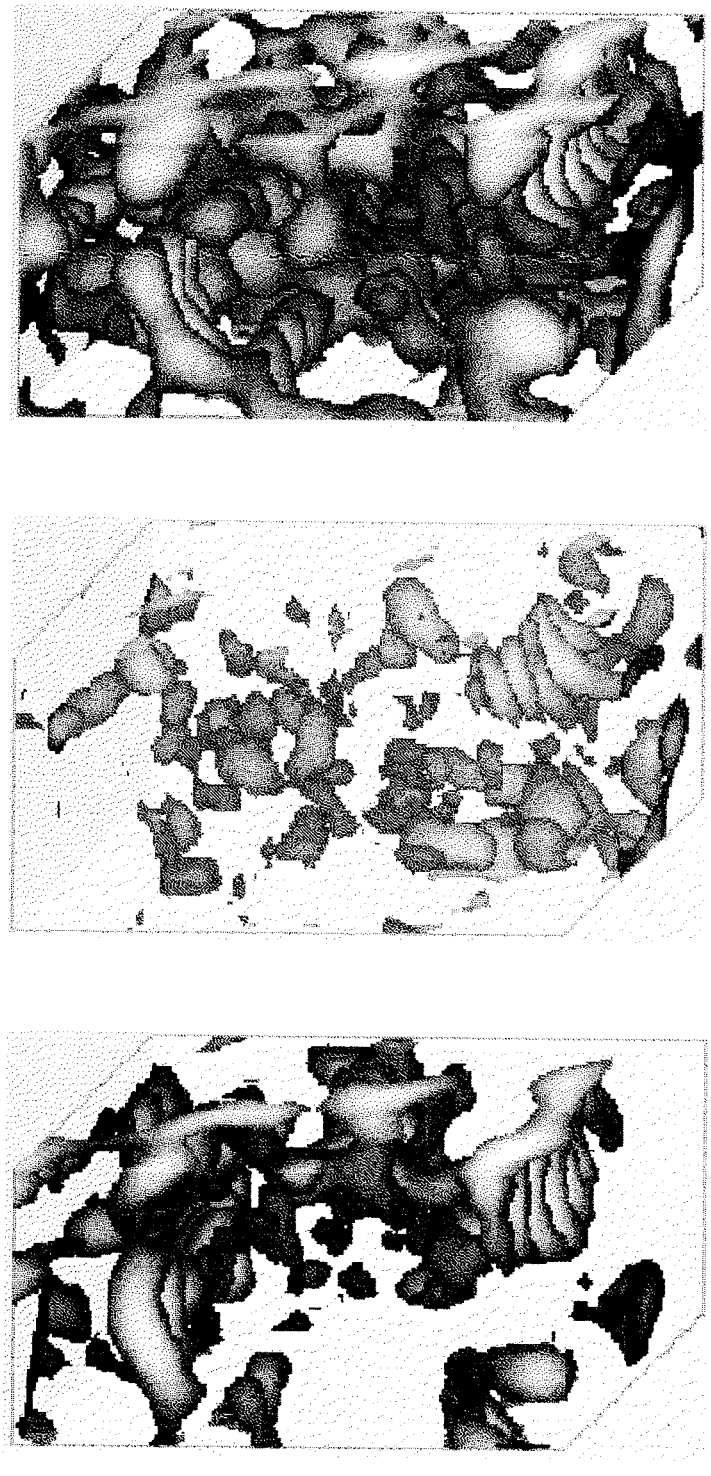

Figure 6. High resolution NMR image of water in Bentheim sandstone at initial oil saturation.

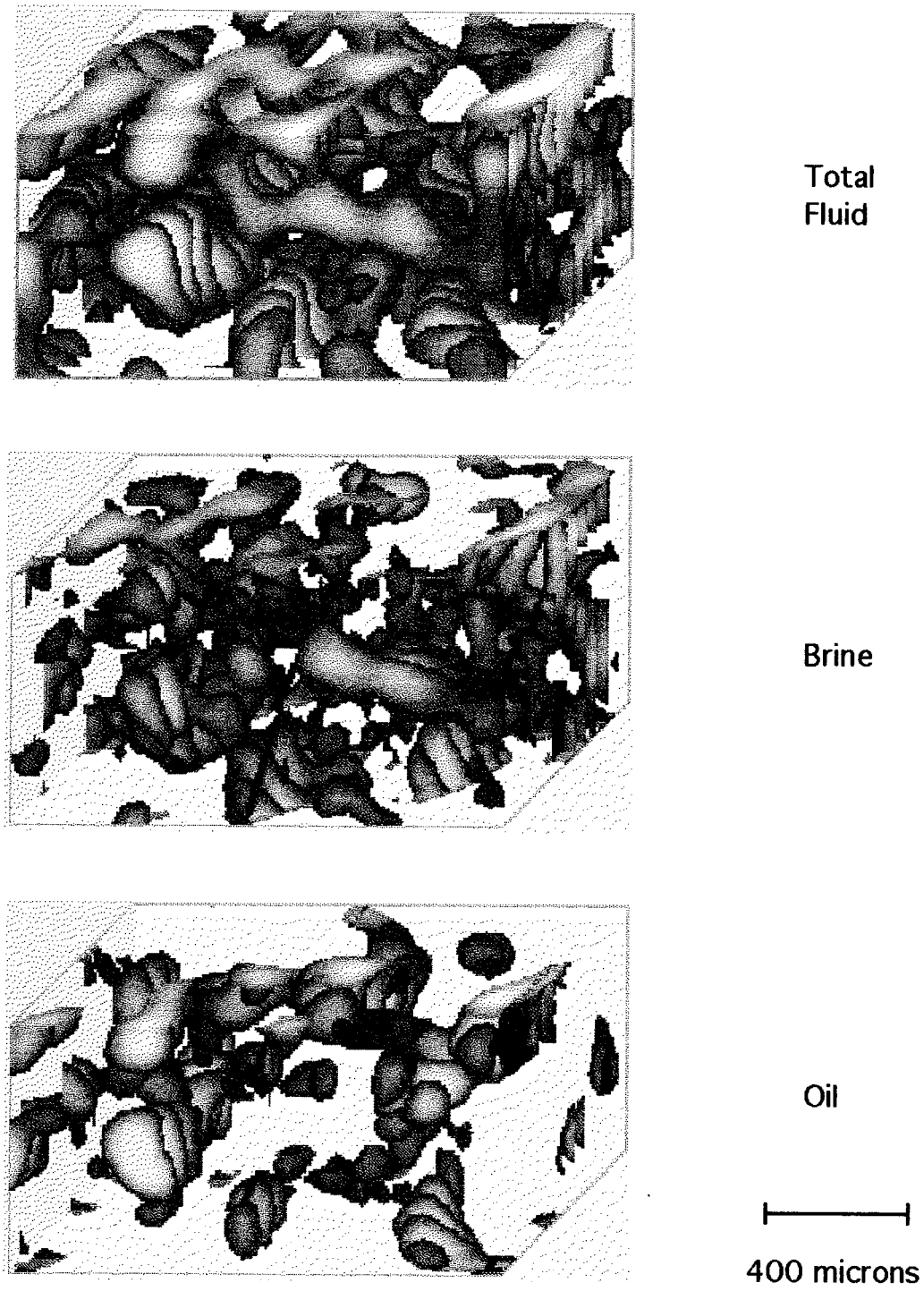

Figure 7. High resolution NMR image of water in Bentheim sandstone at residual oil saturation.

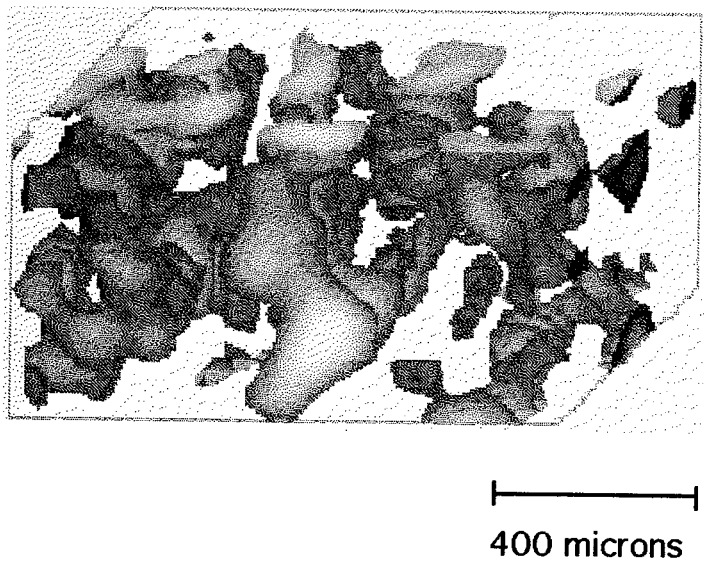

Figure 8. High resolution NMR image of water in Bartlesville sandstone (single phase)